IMPACT OF POSITIONING ERRORS IN THE TWO-MICROPHONE METHOD FOR SURFACE IMPEDANCE MEASUREMENTS

Jonas Heck*, Haoyue Liu*, Lukas Aspöck, Janina Fels, Michael Vorländer

**These authors contributed equally to this work.*

Institute for Hearing Technology and Acoustics, RWTH Aachen University, Germany

Abstract

The two-microphone method, as defined in the standard ANSI/ASA S1.18-2018, is used to determine the acoustic impedance of ground surfaces. To derive the impedance from the sound pressure ratio of the two microphones, the method relies on a specific geometric relationship between the sound source and the two receiving microphones. Therefore, we explore the effect of positioning errors within the measurement setup, i.e. in the alignment between source and receivers.
First, an experiment is conducted to characterize the uncertainties in triaxial geometric positioning that occur during manual setup under practical measurement conditions. The resulting probability distribution is used as input for a Monte Carlo (MC) uncertainty propagation across the template method applying the variable porosity model for a sample material. Consequently, the uncertainty is analyzed for the level difference of the two microphone signals, which is a critical intermediate processing step. The microphone signals are computed by adding the geometrical paths of direct and reflected sound emitted by a point source using the Weyl–Van der Pol approximation for spherical waves. The MC simulation yields the resulting uncertainty estimates for the impedance.
First results show that uncertainty arising solely from geometric setup variations is relatively small but strongly frequency-dependent. The uncertainty of the impedance is larger at low frequencies than at high frequencies. Positioning errors in height show to have the strongest influence on the output quantities.

Keywords: *Surface impedance, measurement, uncertainty*

***Corresponding author**: jonas.heck@akustik.rwth-aachen.de.*

1. Introduction

Acoustic surface impedance is essential for predicting outdoor sound propagation. The two-microphone method (transfer function method) as described in the standard ANSI/ASA S1.18-2018 is one of the few standardized approaches for outdoor ground impedance measurements [1]. In this method, a sound source and two microphones are placed above the ground surface in a prescribed geometry as shown in Fig. 1. The transfer function is obtained from the pressure ratio between the two microphone positions, from which the corresponding level difference (LD) is calculated. The impedance is derived by comparison to a so-called LD template curve (Template method) which is calculated based on impedance models and a specific geometrical setup. Here, we use Geometry A.

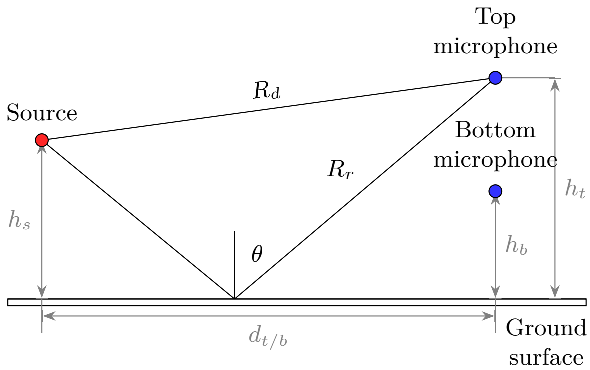

Figure 1: Two-microphone method as in defined ANSI/ASA S1.18-2018. Measurement geometry defined by distance $d_{t/b}$ and height of source and receivers, h_s, h_t and h_b. R_d: direct path between loudspeaker and microphone, R_r: ground-reflected path.

Practical measurements over various grounds have shown considerable variation. This raised the question of how much uncertainty is introduced by the

measurement setup itself and if the result could be accompanied by a quantitative statement of uncertainty. A number of studies deliver important insights regarding the uncertainty factors and stability of the measurement method [2], [3], [4], [5], [6], [7]. Nevertheless, they mainly address selected errors or study cases and do not provide a comprehensive uncertainty analysis of the two-microphone method. In particular, they often use limited spatial resolution and have not experimentally characterized the geometric deviations introduced during manual setup.
This study addresses this gap by investigating deviations from the template geometry experimentally. The aim is to obtain possible source-receiver geometries that represent the measured positioning uncertainty. They are consequently used in a numerical uncertainty propagation to evaluate their influence on the level difference and the complex surface impedance.

2. Methods

2.1. Workflow

The main building blocks of the study are shown in Fig. 2. In order to determine a probability distribution for the perturbed geometries, i.e. the offsets introduced by manual setup, an experiment has been conducted which is presented in Section 3. Each uncertainty propagation has to be conducted for a specific surface characteristic. The selected case for this study is depicted in Section 2.2.
This section further describes how the experimentally determined geometric offset distributions are propagated to the pressure ratio using discrete Monte Carlo (MC) sampling. The idea behind the MC method is to repeatedly sample possible values of the input quantities according to their assigned probability distributions and to evaluate the measurement model for each sampled input vector [8]. The propagation is obtained by simulating virtual microphone signals based on the perturbed geometries. Eventually, the simulated level differences are used to derive the estimated impedance when applying the template method.

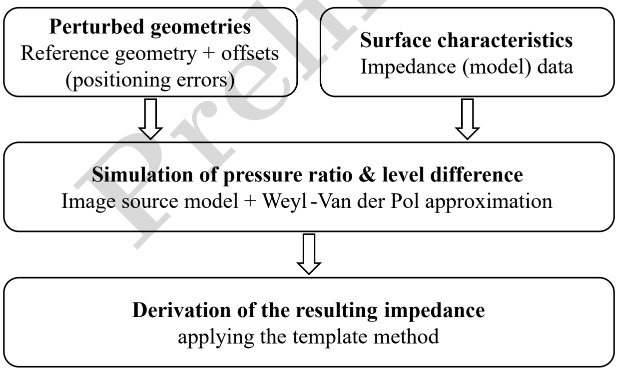

Figure 2: Workflow of the study.

The procedure contains the following steps:

1. **Input distributions:** Each geometric input quantity x_i is described by its experimentally fitted normal distribution, namely the mean and the standard deviation:
$$x_i \sim \mathcal{N}(\mu_{\text{exp},i}, \sigma^2_{\text{exp},i}) \qquad i = 1, \ldots, 9. \quad (1)$$
2. **Sampling range:** For each input quantity, a finite sampling range is defined to cover approximately 99.7% ($\pm 3\sigma_{\text{exp},i}$) of the fitted normal distribution. The lower and upper bounds are rounded to integer millimeter values:
$$x_{\min\,/\,\max,i} = \lfloor \mu_{\text{exp},i} \pm 3\sigma_{\text{exp},i} \rceil \quad (2)$$
3. **Discrete grid:** A discrete grid with a geometric resolution of 1 mm is constructed between the lower and upper bounds, $x_{\min,i}$ and $x_{\max,i}$. Each value in this grid represents one possible geometric value in the Cartesian coordinate system.
4. **Probability evaluation:** The probability density function (PDF) returns a value of the experimentally fitted normal distribution $\mathcal{N}(\mu_{\text{exp},i}, \sigma^2_{\text{exp},i})$ at each grid value x_i:
$$p_i(x_i) = \texttt{pdf}\left(\mathcal{N}(\mu_{\text{exp},i}, \sigma^2_{\text{exp},i}), x_i\right). \quad (3)$$
5. **Probability normalization:** Since the continuous distribution is represented on a discrete grid, the evaluated probability densities are normalized so that the discrete probabilities sum to unity:
$$P_i(x_i) = \frac{p_i(x_i)}{\sum_{x_i} p_i(x_i)}. \quad (4)$$
6. **MC sampling:** A total of M random offset combinations is drawn from the discrete distributions. Each grid value is selected according to its sampling probability $P_i(x_i)$. Each combination contains one sampled offset value for each of the nine geometric input quantities.
7. **Coordinate transformation:** The sampled offset combinations are converted into the corresponding height–distance coordinate variables as described in Figure 1.
8. **Simulation:** For each sampled (perturbed) geometry, the pressure ratio between the top and the bottom microphone is calculated using the image source model and applying the spherical wave approximation by Weyl-Van der Pol [1].

The level difference is calculated with the pressure of the top and bottom microphone $p_t(f)$ and $p_b(f)$ as:
$$LD(f) = 20\log_{10}\left(\left|\frac{p_t(f)}{p_b(f)}\right|\right). \quad (5)$$
The template method uses the level difference as input. The average level difference per virtual/simulated

measurement trial $LD_{m,av}(f)$ is compared with the calculated level difference of the reference geometry $LD_c(f)$:

$$E = \sum_f \left(\frac{LD_c(f) - LD_{m,av}(f)}{\phi(f)} \right)^2 , \qquad (6)$$

where $\phi(f)$ is the standard deviation of the simulated level differences at frequency f.
For the calculation of $LD_c(f)$, a set of model parameters is estimated. Then, the method iterates the model parameters in order to minimize E. The spectrum with the smallest value of E is selected as the best fit for the parameters. Thus, the impedance is taken from the chosen material model.

2.2. Case study: (Virtual/Simulated) Grass

In this present study, we limit our analysis to a case study with the following characteristics:

- Surface material under test: Grass based on the two-parameter (variable porosity) model [9] with flow resistivity $\sigma_e = 152$ kPa $\cdot$ s $\cdot$ m^{-2} and porosity $\alpha_e = -52$ m^{-1}.
- Measurement Geometry A with $d = 1.75$ m, $h_s = 0.325$ m, $h_t = 0.23$ m and $h_b = 0.23$ m.
- Impedance deduction strategy: Template Method.
- Frequency range: $100 - 4000$ Hz, with a linear step size of 10 Hz.
- Possible parameter range for the calculation of LD_c, see Eq. (6):
  - $\sigma_e \in (5, 30 \times 10^3)$ kPa $\cdot$ s $\cdot$ m^{-2},
  - $\alpha_e \in (-100, 100) \times 10^3$ m^{-1}.
- Only one meteorological condition.

3. Positioning errors as geometric input uncertainty

To quantify the uncertainty introduced during the manual setup process, an experiment is conducted involving 22 participants. The resulting data are analyzed to assess setup accuracy and to derive representative geometric offset distributions from the reference geometry.
The experiment uses an infrared-based OptiTrack system with six cameras for position tracking. Infrared light emitted by the camera LEDs is reflected by the reflective markers placed within the measurement area and detected by the cameras to determine marker positions. The markers are connected to mock-ups of the loudspeaker and the two microphones. Attention is given to a high calibration quality near the ground plane, resulting in an triangulation error below 0.5 mm for all possible positions.

The participants are instructed to position three marker mock-ups according to the specified values for the reference Geometry A specified in the ANSI/ASA standard [1]. The instructions provided target values for the loudspeaker height (h_s), the top and bottom microphone heights (h_s and h_s), the horizontal source-receiver separations (d), as specified in Section 2.2. The measurement tools provided consist of a rigid rod used to assist the measurement of the source-to-receiver distance and two folding rulers.
To enable a consistent comparison with the reference geometry, the measured data is transformed into the reference coordinate system, as shown in Fig. 3. The transformation method considers all three positions P_{LS}, P_T and P_B of the loudspeaker and the two microphone mock-ups jointly as a triangle to preserve their geometric relationships. First, the centroid of each measurement setup trial C is translated into the ideal reference centroid C_{ref}. Then, the triangle is rotated around the z-axis such that the vector from the centroid to the loudspeaker is aligned with the corresponding direction in the reference geometry.

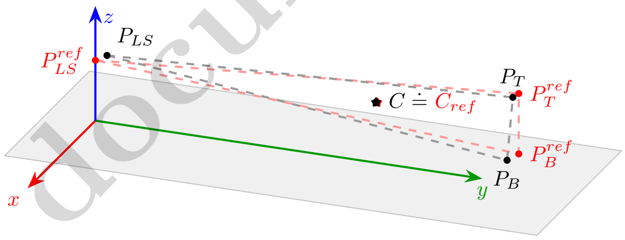

Figure 3: Schematic of the experiment results.

For each of the three axes and for each point, P_{LS}, P_T and P_B, a normal distribution is fitted to the offset between the measured geometry and the reference geometry. The fitting uses a maximum likelihood estimation and provides the mean and standard deviation of the resulting PDF. The distributions are shown in Figure 4. Furthermore, an overall normal distribution is fitted to all offset data across all points and axes. The mean of the fitted distribution, shown in red, is exactly zero.

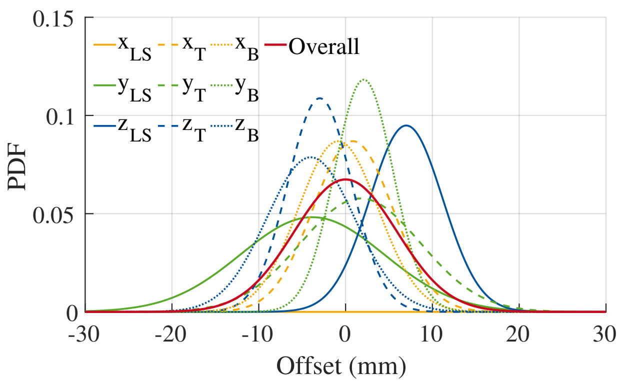

Figure 4: Distribution of the experimental positioning errors for geometry A.

4. Results

4.1. Uncertainty in level difference

The uncertainty propagated from geometric setup to the level difference with 1×10^5 MC trials is shown in Fig. 5 and Table 1. The mean curve in Fig. 5, obtained from the randomly selected trials, and the reference curve, without geometric offset, are very close to each other. This indicates that the resulting uncertainties follow approximately symmetric distributions. This also suggests that, with a sufficiently large number of repetitions, the level difference is statistically insensitive to geometric offsets. The dark gray region corresponds to the 1σ interval containing 68% of the trial results, the gray region represents the 2σ interval containing 95%, and the light gray region represents the 3σ interval containing 99.7% of all trials.

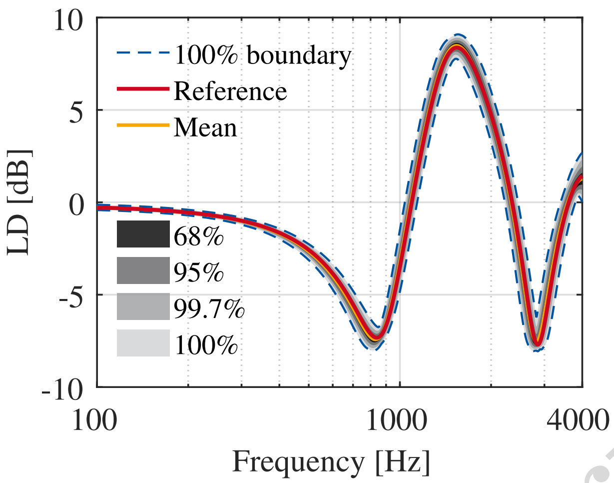

Figure 5: Uncertainty distribution of level difference LD.

The resulting standard uncertainty is presented by the frequency-averaged standard deviation and the maximum value that occurs at a single frequency. The 95% coverage interval is given as an additional measure to describe the spread of the propagated output distribution.

Table 1: Uncertainty statistics of level difference LD.

Quantity	Std. $\sigma(f)$		95 % coverage $W_{95}(f)$	
	Freq.-avg.	Max	Freq.-avg.	Max
LD (dB)	0.33	0.65	1.30	2.53

4.2. Local input sensitivity: Impact of individual positioning errors

To support the interpretation of the MC results, a local input sensitivity analysis is additionally carried out to identify which geometric offsets have the strongest influence on the level difference. Sensitivity coefficients can be obtained numerically by varying one input quantity while keeping the others constant as one-at-a-time finite-difference perturbations [10], [11].

The sensitivity analysis is applied to the nine geometric input quantities x_i defined in Section 2.1. For each input quantity, a positive and a negative perturbation are applied around its reference value $x_i^{+/-} = x_{i,\text{ref}} \pm \Delta x_i$. In this study, the same perturbation magnitude is used for all geometric input quantities. It is selected as the arithmetic mean of the standard uncertainties of all geometric input quantities.

The empirical sensitivity coefficient is calculated as [12]:

$$c_{i,Y}(f) \approx \frac{Y(x_i + \Delta x_i, f) - Y(x_i - \Delta x_i, f)}{2\Delta x_i}, \qquad (7)$$

where $Y(x_i \pm \Delta x_i, f)$ are the output values obtained after positive and negative perturbation of the input quantity x_i. All other input quantities are kept at their reference values during this perturbation.

The sensitivity coefficients resulting from the positioning errors of the loudspeaker and the two microphones are shown in Fig. 6. The z-axis shows the highest local sensitivity, while the x-axis is omitted for clarity due to very small values. Thus, the output quantities are most strongly affected by vertical positioning errors. Among all geometric input quantities, the loudspeaker height has the largest sensitivity.

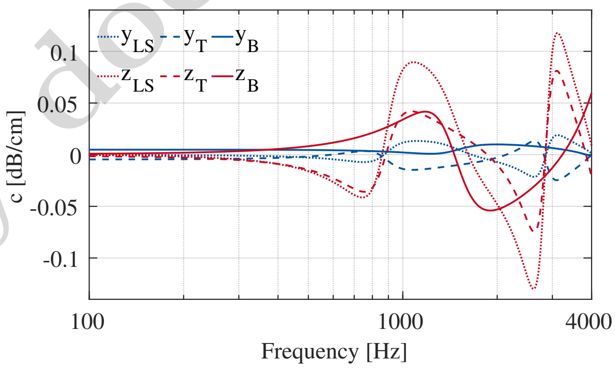

Figure 6: Sensitivity coefficients for level difference LD from loudspeaker, top and bottom microphone positioning errors in y- and z-direction. Offsets in x-direction are omitted; they show very little sensitivity.

4.3. Uncertainty in impedance

The uncertainty of impedance as it results from the MC method with 3×10^5 trials is shown in Figure 7, Figure 8 and Table 2. The mean curves in Figure 7 and Figure 8 refer to the values averaged over all results, which are not necessarily the result of a physically existing geometry.

For both the real and the imaginary part of the impedance, the uncertainties are larger at low frequencies and decrease toward higher frequencies. The mean of $\Re(\mathbf{Z})$ closely follows the reference curve over most of the frequency range, whereas the mean of $\Im(\mathbf{Z})$ shows a larger deviation at low frequencies before approaching the reference at higher frequencies. This suggests that individual trials can deviate noticeably from the reference, particularly in the low frequency range, while the averaged result remains more stable and representative of the reference behavior.

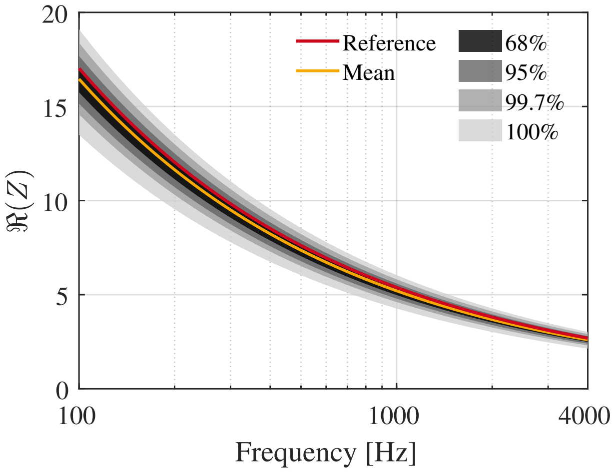

Figure 7: Uncertainty distribution of the real part of impedance $\Re(\mathbf{Z})$.

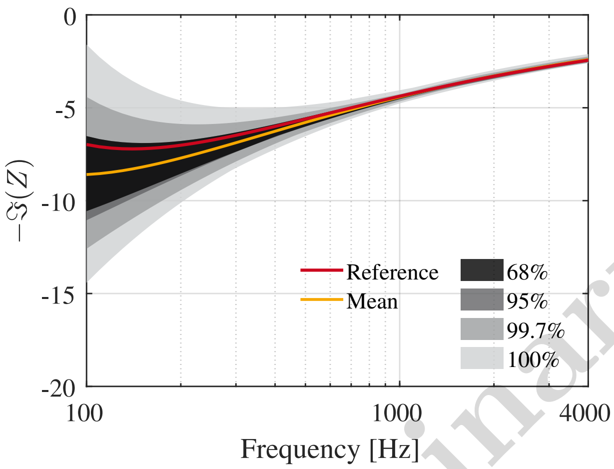

Figure 8: Uncertainty distribution of the imaginary part of impedance $\Im(\mathbf{Z})$.

Table 2 shows that the frequency-averaged uncertainties are relatively small, whereas the maximum reveals pronounced outliers. This again confirms that uncertainty shows a strong frequency dependence.

Table 2: Uncertainty statistics for impedance **Z**.

Quantity	Std. $\sigma(f)$		95 % coverage $W_{95}(f)$	
	Freq.-avg.	Max	Freq.-avg.	Max
$\Re\{\mathbf{Z}\}$	0.16	0.57	0.69	2.53
$\Im\{\mathbf{Z}\}$	0.12	1.57	0.37	4.53

5. Conclusion and outlook

The experimental characterization of source and receiver positioning errors provides realistic probability distributions for the geometric input parameters. These distributions form the basis of the uncertainty propagation and represent a practical alternative to the assumed input distributions commonly adopted in previous studies [4], [13]. The fitted normal distributions show standard deviations ranging from approximately 3.4 to 8.3 mm for Geometry A. A linearized sensitivity analysis further indicates that microphone height is the dominant geometric input parameter affecting level difference.

The propagation from geometric uncertainty to level difference and impedance was evaluated. The results indicate that geometric offsets mainly introduce frequency shifts in the level difference curve, whereas the overall curve shape remains comparatively stable. This suggests that the overall shape of the level difference curve is more important for surface characterization using the template method than the exact frequency locations of individual peaks and dips. The averaged impedance remains close to the reference impedance, indicating that geometric offsets do not introduce a noticeable systematic bias under the investigated conditions. However, the uncertainty is strongly frequency-dependent and differs between the real and imaginary parts of the impedance. For the template method, the largest impedance uncertainties occur in the low-frequency region for both the real and imaginary parts. Despite these variations, the overall shape of the impedance curve remains preserved.

The statistical uncertainty analysis and the boundary analysis describe geometric uncertainty from different perspectives. While the statistical analysis describes the expected variability under realistic measurement conditions, the boundary analysis identifies the maximum deviations within the prescribed geometric limits. It should be noted that the range of uncertainty can become significantly larger for individual “worst case” geometries than for a MC trial with repeated measurements.

Overall, the results show that geometric uncertainty can be a relevant contributor to the uncertainty of acoustic impedance measurements and should be considered when interpreting surface impedance results. The presented framework provides a quantitative basis for assessing this influence and for evaluating measurement strategies aimed at reducing uncertainty. For the investigated example, however, the resulting uncertainties remain moderate. This suggests that the impedance deduction procedures are reasonably robust against typical geometric positioning errors. Although the geometric uncertainty causes noticeable deviations in the intermediate level difference results, its effect on the final impedance is less pronounced.

6. Outlook

Future work will extend the uncertainty analysis to other surface types, impedance models, and source–receiver geometries. This would help assess whether the trends observed for the selected grass surface and measurement configuration also apply under different conditions. The ANSI/ASA standard describes the direct method as an alternative to derive

the impedance without using parameterized material models. This approach might lead to a different uncertainty propagation behavior.
Additional uncertainty sources can also be incorporated into the propagation framework, e.g. sensor calibration, source directivity, atmospheric variability, background noise, and spatial inhomogeneity of the ground surface. Furthermore, the error function function used in the template method could be investigated in more detail. Possible improvements, e.g. shift correction, derivative-based similarity measures or alternative weighting strategies, may help to distinguish curve shape differences for critical frequencies more effectively than broad frequency-band averaging.

References

[1] ANSI/ASA S1.18, *Method for determining the acoustic impedance of ground surfaces*, Acoustical Society of America, 2018.

[2] R. Kruse, "Application of the two-microphone method for in-situ ground impedance measurements," *Acta Acustica united with Acustica*, vol. 93, no. 5, 2007.

[3] R. Kruse, V. Mellert, and P. Rong, "Optimized geometry for ground impedance measurement," *The Journal of the Acoustical Society of America*, vol. 121, no. 5_Supplement, May 2007. DOI: 10.1121/1.4781653

[4] R. Kruse and V. Mellert, "Effect and minimization of errors in in situ ground impedance measurements," *Applied Acoustics*, vol. 69, no. 10, Oct. 2008. DOI: 10.1016/j.apacoust.2007.05.010

[5] C. Liu, "Impedance deduction for vegetated roof surfaces: Multiple geometry strategy," in *INTER-NOISE and NOISE-CON Congress and Conference Proceedings*, Institute of Noise Control Engineering, vol. 253, 2016, pp. 3299–3305.

[6] C. Liu, F. Georgiou, and M. Hornikx, "Influence of transducer locations on acoustic impedance prediction in porous systems with application to vegetated roofs," *Applied Acoustics*, vol. 246, pp. 111–213, Mar. 2026. DOI: 10.1016/j.apacoust.2025.111213

[7] T. Van Renterghem, F. Huyghe, and K. Verheyen, "Effect of tree species and season on the ability of forest floors to abate environmental noise," *Applied Acoustics*, vol. 184, Dec. 2021. DOI: 10.1016/j.apacoust.2021.108349

[8] JCGM 101, *Evaluation of measurement data – supplement 1 – propagation of distributions using a monte carlo method*, Joint Committee for Guides in Metrology, 2008.

[9] K. Attenborough, "Acoustical impedance models for outdoor ground surfaces," *Journal of Sound and Vibration*, vol. 99, no. 4, pp. 521–544, 1985. DOI: 10.1016/0022-460X(85)90538-3

[10] ISO/IEC Guide 98-3, *Guide to the expression of uncertainty in measurement (gum:1995)*, International Organization for Standardization, 2008.

[11] JCGM 100, *Evaluation of measurement data – guide to the expression of uncertainty in measurement*, Joint Committee for Guides in Metrology, 2008.

[12] B. Taylor, *Methodus incrementorum directa & inversa.* 1715.

[13] E. Brandao, R. C. Flesch, A. Lenzi, and C. A. Flesch, "Estimation of pressure-particle velocity impedance measurement uncertainty using the monte carlo method," *The Journal of the Acoustical Society of America*, vol. 130, no. 1, EL25–EL31, 2011. DOI: 10.1121/1.3601882